Nuclear Instruments and Methods in Physics Research B xxx (2017) xxx–xxx

Contents lists available at ScienceDirect

Nuclear Instruments and Methods in Physics Research B

journal homepage: www.elsevier.com/locate/nimb

Microstructural, mechanical and optical properties research of a carbon ion-irradiated Y_2SiO_5 crystal

Hong-Lian Song [a], Xiao-Fei Yu [a], Qing Huang [b], Mei Qiao [a], Tie-Jun Wang [a], Jing Zhang [a], Yong Liu [a], Peng Liu [a], Zi-Hua Zhu [c], Xue-Lin Wang [a,*]

[a] School of Physics, State Key Laboratory of Crystal Materials and Key Laboratory of Particle Physics and Particle Irradiation (MOE), Shandong University, Jinan 250100, PR China
[b] Shanghai Institute of Applied Physics, Chinese Academy of Sciences (CAS), Shanghai 201800, PR China
[c] Environmental Molecular Sciences Laboratory, Pacific Northwest National Laboratory, Richland, WA 99354, USA

ARTICLE INFO

Article history:
Received 9 August 2016
Received in revised form 17 December 2016
Accepted 18 January 2017
Available online xxxx

Keywords:
Y_2SiO_5
Ion irradiation
SIMS
Raman
Optical

ABSTRACT

Ion irradiation has been a popular method to modify properties of different kinds of materials. Ion-irradiated crystals have been studied for years, but the effects on microstructure and optical properties during irradiation process are still controversial. In this paper, we used 6 MeV C ions with a fluence of 1×10^{15} ion/cm^2 irradiated Y_2SiO_5 (YSO) crystal at room temperature, and discussed the influence of C ion irradiation on the microstructure, mechanical and optical properties of YSO crystal by Rutherford backscattering/channeling analyzes (RBS/C), X-ray diffraction patterns (XRD), Raman, nano-indentation test, transmission and absorption spectroscopy, the prism coupling and the end-facet coupling experiments. We also used the secondary ion mass spectrometry (SIMS) to analyze the elements distribution along sputtering depth. 6 MeV C ions with a fluence of 1×10^{15} ion/cm^2 irradiated caused the deformation of YSO structure and also influenced the spectral properties and lattice vibrations.

1. Introduction

In recent years, yttrium mono-silicate Y_2SiO_5 (YSO) gained much attention as a potential material for wide range of applications because of their special properties, such as high temperature strength, chemical resistance, low thermal expansion, visible light transparency, high conductivity and mechanical compatibility [1–5]. YSO can be found in two different monoclinic structures: X_1-YSO and X_2-YSO, which are the low temperature phase and high temperature phase, respectively [6]. In the preparation process of X_2 structure YSO crystal, the temperature is usually more than 1200 °C, at which only a few nano-structure materials can keep stability. So most studies about YSO nano-structure are focus on the X_1 structure [7,8]. Due to chemical and thermo-mechanical properties, Er^{3+} doped YSO has been investigated for solid-state laser application [9]. Due to their strong luminescence and highly saturated color, Tb^{3+} and Ce^{3+} doped YSO are well known phosphor materials used in cathode ray tubes, field emission displays and fluorescent lamps [10]. Therefore, YSO is an ideal host material for optical devices because of its advantages.

The ion irradiation technique which differs from proton exchange or Ti in diffusion is proved to be a promising method to modify surface properties due to the accurate control of dopant composition and structure modification [11–13]. Up to now, the ion irradiation technique has been successfully used to form waveguide structure in more than 100 materials, which including glasses, crystal and polymers [14,15]. The mechanical, optical, electronic and chemical properties of YSO strongly lie on its crystal structure, which can be easily modified in an irradiation environment [16–18]. G. Corriellia et al. fabricated waveguide in Pr^{3+}: YSO crystal by femtosecond-laser micromachining [19]. To the best of our knowledge, there are few studies on the effect of carbon ion irradiation of the YSO crystal. Therefore, the research on the performance of YSO in an irradiation environment and applications of property modification by ion irradiation still needs further insight compared with other materials such as metals and semiconductors [14,15]. This work is the first time to discuss the influence of C ion irradiation on the microstructure, mechanical and optical properties of YSO crystal and report the formation of a planar optical waveguide in YSO crystal by using 6 MeV C ions with a fluence of 1×10^{15} ion/cm^2.

* Corresponding author.
E-mail address: xuelinwang@sdu.edu.cn (X.-L. Wang).

http://dx.doi.org/10.1016/j.nimb.2017.01.038
0168-583X/

2. Experiment and methods

The YSO crystals we used in experiments were grown by the Czochralski technique in a RF-heating apparatus heated iridium crucible with Y_2O_3 and SiO_2 as the raw materials. The melting point is about 2000 °C. The ion irradiation process was carried out at 2 × 1.7 MV tandem accelerator within State Key Laboratory of Nuclear Physics and Technology, Peking University, and subsequently, the microstructural, mechanical and optical properties were studied. Comparing with this irradiated sample, we prepared a virgin sample of YSO for the same tests. To study the composition of the irradiated sample, secondary ion mass spectrometry (SIMS) experiments was carried out with a Time-of-Flight Secondary Ion Mass Spectrometry (ToF-SIMS) at Pacific Northwest National Laboratory (PNNL), which can show the elements distribution along the depth. The SRIM (stopping and range of ions in matter) software was used to see the energy deposition and ion distribution, which can be compared with the results of SIMS tests. Two samples were characterized by Rutherford backscattering/channeling analyzes (RBS/C) using 2 MeV He^+ ions as the probing beam delivered by a 2 × 1.7-MV tandem accelerator at a backscattering angle of 160°. The XRD spectra were performed by X-ray diffraction (XRD) using Cu Kα radiation with a Rigaku RINT-2500VHF and HRXRD measurements were performed on a Bruker AXS HRXRD D5005 system (λ = 1.54056 Å). The Raman spectra were measured using a confocal Raman system (Bruker SENTERRA dispersive Raman microscope) with 532 nm, 633 nm and 785 nm excitation wavelength. The nano-indentation measurement (hardness and elastic (Young's) modulus) was performed using an Agilent Technologies G200 Nano Indenter. To study the optical properties of two samples, the transmission and absorption spectra were measured using a UV–Vis spectrometer; and the effective refractive index profiles were got from the dark mode spectra which were measured with a Metricon 2010 prism coupler (Metricon Corporation, USA); the end-facet coupling experiments were carried out to get the near-field intensity distribution profiles. The XRD spectra, Raman spectra and nano-indentation measurement were measured to study the microstructure of the irradiated sample.

3. Results and discussion

Secondary ion mass spectrometry is proved to be a promising technique to analyze the composition of materials, including not only solid materials but some liquid materials [20,21]. By sputtering the surface of samples, SIMS can analyze the elements distribution along sputtering depth. In this paper we used SIMS technique to explore the irradiated carbon ion distribution. During the experimental process, bismuth was used as the analyzing ion source while the caesium was used as sputtering ion source. As shown in Fig. 1(a), the orange line shows carbon ions distribution. To exhibit the carbon ion distribution more clearly, a black line was got after smoothing the orange line. These two lines are related with right Y-axis while the others are related with left Y-axis. In Fig. 1 (a), we can clearly see the carbon ion distribution along the irradiated depth. The C-ions intensity reaches maximum value at the depth of about 4 μm, which means most of the incoming C ions gathered at the depth of 4 μm. Because of the gathering of the incoming C ions, the volume of this area increased, which resulted in the decrease of refractive index as shown in Fig. 7(a) and a "barrier" was formed restricting the propagation of the light.

It is well known that SRIM [22] is a very powerful tool to simulate the physical process of ion irradiation and analyze the formation mechanism of the waveguide. We simulated the process of 6 MeV C ions irradiation on YSO crystal and calculated nuclear (S_n) and electronic (S_e) stopping power profiles as shown in Fig. 1 (b). From Fig. 1(b), at the sample surface, energy deposition is dominated by the electronic (S_e) stopping power and simultaneously, the nuclear (S_n) stopping power occupies a dominate position at the end of ion trajectory. The peak position of S_n is approximately 4 μm, which is in agreement with the SIMS result (as shown in Fig. 1(a)). It can be seen that the nuclear stopping power are the main reason for lattice damage in the crystal, which results in a decrease in the physical density and lead to a reduced refractive index.

The measured RBS/C spectra of YSO crystal irradiated by 2.0 MeV He ions both along and at 7° off channeling direction to detect the damage in the waveguide are shown in Fig. 2. For comparison, the random and virgin spectra of the virgin YSO sample are also measured. We also used SIMNRA to simulate the random spectra, which clarify the signals of Y, Si and O atoms. The damage spectra of ion irradiated YSO sample is different from the virgin spectra and lower than the random spectra. The damage ratio (f_d) in the surface region corresponding to the channel number of 428 can be calculated by a classical approximate expression [23]:

$$f_d = x_i - x_v / x_r - x_v \quad (1)$$

where x_i, x_r and x_v are the backscattering yields of the irradiated YSO sample in channeling condition, the virgin sample in a random orientation and in channeling condition, respectively. The damage ratio $f_{d,sur}$ of the sample surface is about 0.026. The result shows that there are some atom displacement from lattice sites and some atomic rearrangement after C ion irradiation.

Fig. 3 shows XRD pattern of virgin YSO crystal samples (0 1 0), which were in agreement with the standard JCPDS card of X_1-Y_2SiO_5 with lattice constant a = 10.41 Å, b = 6.73 Å and c = 12.46 Å (NO. 21-1458). In order to accurately determine the irradiation-induced peak evolution, we measured the HR-XRD

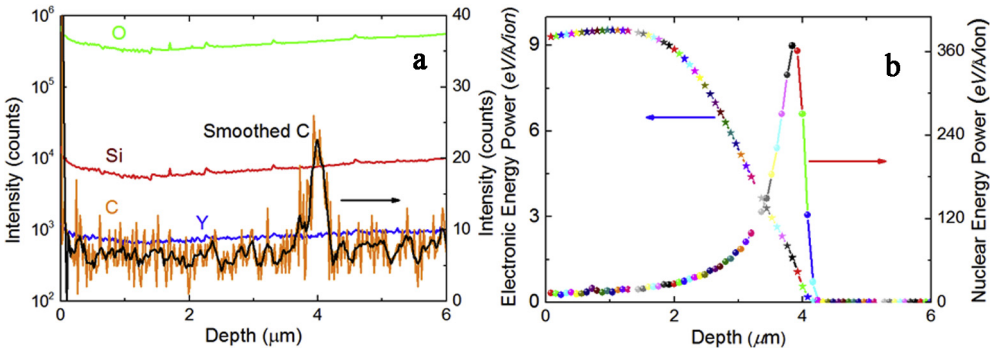

Fig. 1. (a) The secondary ion mass spectrometry (SIMS) spectra show the elements distribution along the depth; (b) the electronic and nuclear stopping power deposition as function of penetration depth of 6 MeV C ions irradiated YSO waveguide simulated by the SRIM 2010.

Please cite this article in press as: H.-L. Song et al., Microstructural, mechanical and optical properties research of a carbon ion-irradiated Y_2SiO_5 crystal, Nucl. Instr. Meth. B (2017), http://dx.doi.org/10.1016/j.nimb.2017.01.038

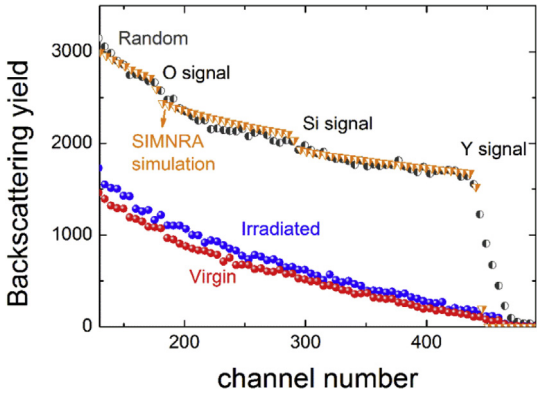

Fig. 2. RBS/C and SIMNRA simulation spectra of YSO crystal irradiated by 6 MeV C ions with the fluence of 1×10^{15} ion/cm^2 both along and at 7° off channeling direction at room temperature.

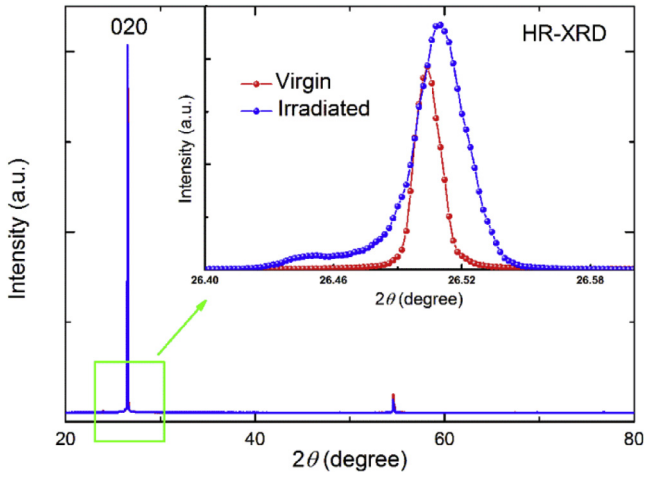

Fig. 3. XRD pattern of the virgin and irradiated YSO crystal samples, the inset showing the HR-XRD pattern of (020) peak.

spectra as shown in the inset of Fig. 3, the result shows that the orientation of YSO sample did not change after C ion irradiation. The average crystallite size of the samples is calculated according to the Debye-Scherer equation [24]:

$$D = \frac{k\lambda}{\beta \cos\theta} \tag{2}$$

where D is the average crystallite size, k is a constant of 0.9, λ is the X-ray wavelength (λ = 1.54056 Å), β is the full width at half maximum (FWHM), and θ is the Bragg angle of the (020) peak. Table 1 shows different parameters obtained from the HR-XRD spectra and Eq. (2).

It is evident from the Table 1 that the FWHM of C ions irradiated sample was broader than virgin YSO sample and the peak position shifted toward to higher 2θ values, which indicates a compressive strain in the near surface damage region has been confirmed owing to the C incorporation [25,26]. The (020) peak broadening in the HR-XRD pattern after C ion irradiation also reveals that a slight reduction of the crystalline coherence length through the creation of vacancies and dislocations in the surface of irradiated sample [27]. Fig. 3 shows that the intensity of the (020) peak of irradiated YSO increases considerably with an increase in the FWHM (from 0.013 to 0.024) and a hump appeared near the (020) peak, which suggests a slight amorphization of the irradiated YSO sample [28]. After C ion irradiation, the average particle size is reduced from 13.78 to 7.49 nm in diameter. The reduction in the crystallite size is mainly due to the distortion in the YSO lattice by the foreign impurity C irradiation, which decrease the nucleation and subsequent growth rate by the addition of C ion concentrations [29]. It also indicates that C ion irradiation induced re-crystallization processes may lead to the slight change of crystal lattice in the sample, which is one of the reasons why (020) peak position shifted toward to higher 2θ values. It is evident that there are broadening and a small shift in HR-XRD (020) peak, increase of the intensity of (020) peak and reduction in the particle size in C ions irradiated YSO sample comparing to virgin sample, which indicates that the microstructure of YSO sample is affected by C ions irradiation.

The Raman scattering method is a good way to measure molecular vibration and ion irradiation induced defects [30]. Fig. 4 shows the Raman spectra of the virgin and C ions irradiated YSO sample with 532 nm, 633 nm and 785 nm excitation wavelengths over a frequency range of 50–2000 cm^{-1}. For $(SiO4)^{4-}$ tetrahedron, the T_d (point group symmetry) has nine normal vibrations, and the nine vibrations consist of four fundamental distinguishable modes: V_1 (A) (887 cm^{-1}) the Raman active symmetric stretching vibration, V_2 (E) (399 cm^{-1}) the Raman active doubly degenerate bending vibration, V_3 ($F2$) (905 cm^{-1}) the Raman active triply degenerate anti-symmetric stretching vibration and V_4 ($F2$) (562 cm^{-1}) the Raman active triply degenerate bending vibration [31]. As shown in Fig. 4(a) (532 nm excitation), the peak intensity increased and broadened at 399 cm^{-1} after C ion irradiation. This is attributed to the V_2 (E) active doubly degenerate bending vibration of the $(SiO4)^{4-}$ tetrahedron which results from the lattice deformation and mixed crystal disorder after C ion irradiation. However, a low intensity band is observed in the Raman spectra irradiation at 399 cm^{-1} shown Fig. 4(b) (633 nm excitation), which is because part of the photo-transformed component is reduced [32]. For YSO sample, the most attractive bands is 880–940 cm^{-1}, which corresponds to the V_3 (880–1000 cm^{-1}) active triply degenerate anti-symmetric stretching vibration of the SiO_4 groups. In the Raman spectra of Fig. 4(b), two bands are observed at 887 cm^{-1}, 905 cm^{-1}. Those bands are assigned to the active triply degenerate anti-symmetric stretching mode (V_3) of the $(SiO_4)^{4-}$ tetrahedron. We also found a low intensity band at 958 cm^{-1}, which may be correlated with the V_3 band. After irradiation, the intensity of the 905 cm^{-1} and 958 cm^{-1} band increased as shown in Fig. 4(b). The V_3 active triply degenerate anti-symmetric stretching mode is attributed to the Si–O bridging bond. A mixed stretching mode of the Si–O bridging bond with C ion doped may be caused the intensity change at 905 cm^{-1}.

Series of emission bands were observed in near-infrared regions (800–920 nm) in Fig. 4(c). According to Raman mechanism, this phenomenon should be due to the 785 nm laser induced luminescence effect during the measurement. The signals at 1250 cm^{-1}, 1423 cm^{-1}, 1506 cm^{-1}, 1648 cm^{-1} and 1780 cm^{-1} could shift to the signal of 870 nm, 883 nm, 890 nm, 901 nm and 912.5 nm, respectively. Those signals are equivalent to the partial luminescence bands of YSO crystal by 785 nm laser irradiation. After C ions irradiation, the intensity of 883 nm band has a slightly increase, which could be due to the presence of density of defects [33]. 6 MeV C ions with a fluence of 1×10^{15} ion/cm^2 irradiated caused the deformation of YSO structure and also influenced the spectral properties and lattice vibrations.

To discover the mechanical properties of the irradiated sample, nano-indentation test was performed by using the Agilent Technologies G200 Nano Indenter. A Berkovich diamond indenter tip was used to do the Continuous stiffness measurement (CSM) on the surfaces of the samples. The CSM option allows the continuous measurement of the contact stiffness during loading. This is accomplished by superimposing a small oscillation (with an amplitude of 2 nm in our measurements) on the primary loading signal.

Please cite this article in press as: H.-L. Song et al., Microstructural, mechanical and optical properties research of a carbon ion-irradiated Y_2SiO_5 crystal, Nucl. Instr. Meth. B (2017), http://dx.doi.org/10.1016/j.nimb.2017.01.038

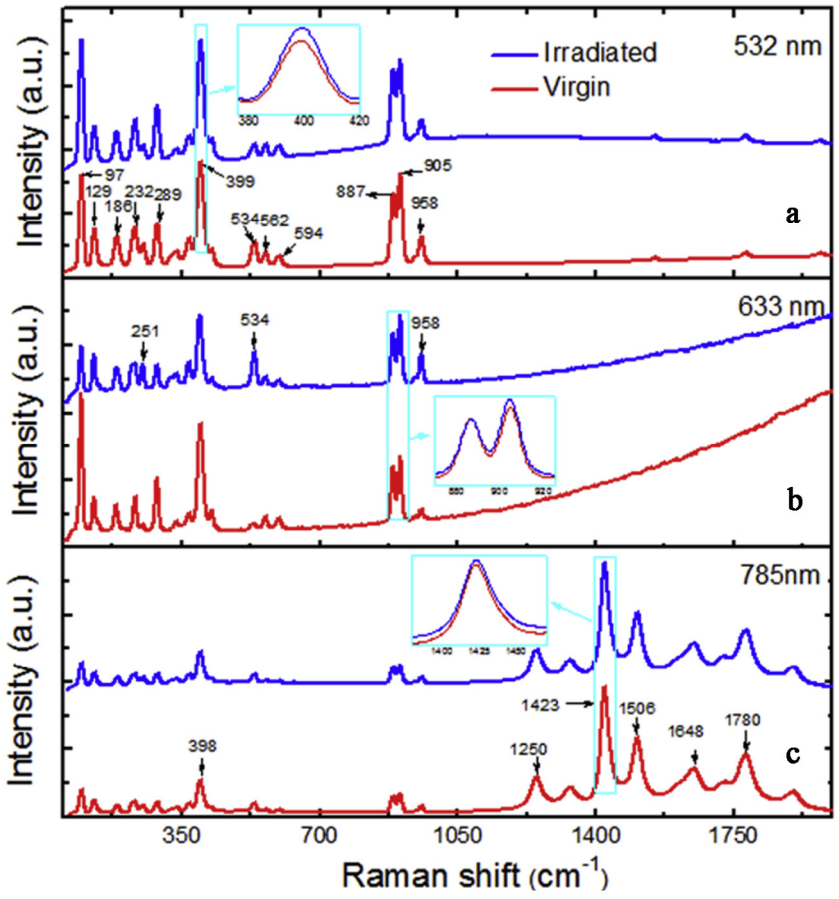

Fig. 4. The Raman spectra of the virgin and irradiated YSO crystal samples over a frequency range of 50–2000 cm^{-1} were recorded using (a) 532 nm, (b) 633 nm and (c) 785 nm excitation laser source at room temperature.

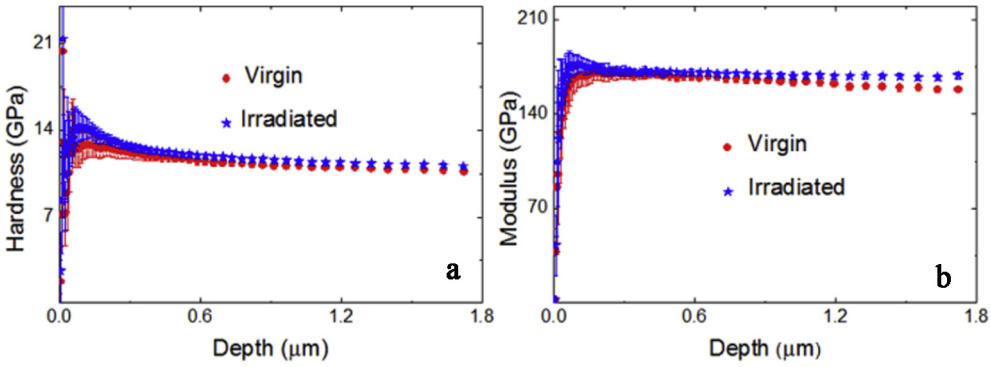

Fig. 5. (a) The hardness and (b) elastic (Young's) modulus as continuous functions of depth were measured based on nano-indentation test utilizing Oliver-Pharr method.

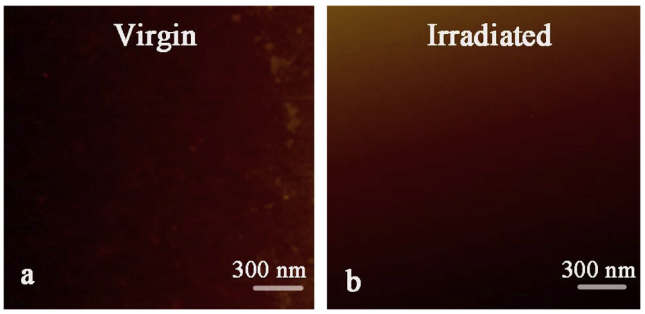

Fig. 6. (a and b) AFM images corresponding to virgin and irradiated YSO samples.

With a continuous measure of contact stiffness, one obtains the hardness and elastic modulus as a continuous function of depth from a single indentation test. But the nano-indentation test could not provide a measurement of the true hardness or modulus at each depth. The reason is that the stress field induced by the indenter extends much deeper than the contact depth. Sixteen indents were measured for each sample to obtain an average hardness and modulus. The distance between indentations was set to be 50 μm.

As shown in Fig. 5(a), the hardness of the irradiated sample is higher than that of the un-irradiated sample, which was ascribed to irradiation-induced interstitials and defect clusters, acting as pinning centers of dislocations [34]. Meanwhile, the elastic modu-

Please cite this article in press as: H.-L. Song et al., Microstructural, mechanical and optical properties research of a carbon ion-irradiated Y_2SiO_5 crystal, Nucl. Instr. Meth. B (2017), http://dx.doi.org/10.1016/j.nimb.2017.01.038

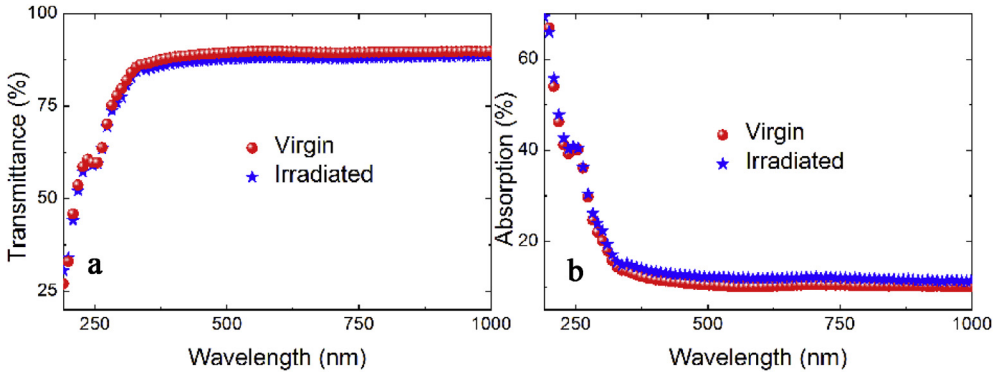

Fig. 7. (a) Transmission and (b) absorption spectra of virgin and irradiated YSO sample recorded over the wavelength range of 190–1000 nm.

Table 1
Different parameters obtained from HR-XRD spectra of virgin and irradiated YSO sample.

Samples	2θ (°)	FWHM (°)	D (nm)
Virgin	26.504	0.013	13.78
Irradiated	26.511	0.024	7.49

lus of the irradiated sample (as shown in Fig. 5(b)) is higher than that of the un-irradiated sample. The chemical bond energy can affect the elastic modulus in materials, which means higher chemical bonds energy leads to higher elastic modulus value [35]. During the C ion irradiation, some Si–O chemical bonds were replaced by C–O chemical bonds which have higher bond energy, giving the result of the slight increase of elastic modulus after irradiation.

The ion irradiation could cause surface roughness and surface microstructure changes during the irradiation process. With different irradiation energies, the sputtering efficiency would change obviously. In the energy range from hundreds of eV to tens of keV, the irradiation would cause significant surface sputtering effect, while irradiation with energy of less than one hundred eV or more than one hundred keV would only cause slightly sputtering influence on the sample surface. The irradiation energy is 6 MeV during our experiments, which means the sputtering effect and induced morphology modification on YSO surface would be extremely weak. As shown in Fig. 6, the average roughness of origin and C-irradiated YSO samples keeps below 0.4 nm, and the surface of YSO crystal could still remain the original optical flatness after ion irradiation process.

We measured the transmission and absorption spectra of the virgin and irradiated YSO sample to better understand the optical properties, As shown in Fig. 7(a), after irradiation, the transmittances are about 88% in the visible and infrared region, which decreased 2% than the virgin sample. In the process of irradiation, YSO crystal can form color centers, which affect the transmission coefficient [11]. Transmission spectra and absorption spectra have almost the same shapes before and after irradiation as shown in from Fig. 7. But it is noted that there are two absorption peaks in 249 nm and 340 nm and the absorbance decreases, the reason for this phenomenon may be due to the lattice defects and the decrease of photon energy in the ultraviolet region. Absorption spectra are almost the same in the visible and infrared regions (as shown in Fig. 7(b)). We can conclude that the absorption is barely affected by C ions irradiation in the visible and infrared regions. The result shows that the C ion irradiation had influence on the absorption in the ultraviolet region but almost no influence on the visible and infrared regions.

We performed the prism coupling measurements of the C ions irradiated YSO sample at a wavelength of 633 nm at room temperature. The refractive index profile is an important parameter in the waveguide and occupies a unique position in devices with practical applications. Fig. 8(a) shows the measured n_{eff} of TE and TM guided modes. For comparison, the substrate refractive index (n_{sub}) of the virgin YSO sample at the wavelength of 633 nm is also shown in Fig. 8(a). We can see from Fig. 8(a), the n_{eff} of TM_0 mode and TE_0 mode after C ions irradiation is 1.78034 and 1.80315, respectively, which are lower than the refractive index of the substrate. According to the results of SIMS and SRIM simulated, the volume of irradiation area increased, which results in a decrease in the physical density and lead to a reduced refractive index after C ions irradiation. This demonstrates that 6 MeV C ions irradiation process will reduce the refractive index and the "barrier" type waveguide could be formed. Fig. 8(b) and (c) shows the 2D near-field intensity distribution for TE_0 and TM_0 polarized light in the waveguide by the end-face coupling method at a wavelength of 633 nm, which were collected by a CCD camera at the output face of the polished waveguide. As shown in Fig. 8(b) and (c), the light could be well confined in the YSO planar waveguide in the visible band. Compared with the measured result of Fig. 8(b), there is almost no light in the air area and substrate layer in Fig. 1(c), which indicates a better confinement of TM_0 polarized light between the surface and the optical barrier. The width of the waveguide was approximately 3.9 μm, which is in agreement with the SIMS and SRIM simulate results.

4. Conclusions

In summary, we studied the microstructure, mechanical and optical properties induced by C ions irradiation utilizing transmission and absorption spectroscopy, X-ray diffraction patterns, Raman patterns, nano-indentation text, and fabricated a "barrier" type planar waveguide structure in YSO crystal by 6 MeV C ion irradiation at a fluence of 1×10^{15} ion/cm^2 at room temperature. The elements distribution along sputtering depth was obtained by SIMS analyze, the volume increased duo to C ion irradiation leads to the decrease of refractive index. Through RBS/C spectra we studied the disorder fraction profile in irradiated YSO crystal and discussed the related irradiation damage through XRD and Raman spectra. From nano-indentation measurement, the increase of hardness and elastic modulus were observed, which means the mechanical properties were changed after ion irradiation. According to the absorption spectra, C ion irradiation had influence on the absorption in the ultraviolet region but almost no influence on the visible and infrared regions. The near-field intensity distribution profiles of the TE and TM guided modes in the visible region (633 nm) are measured, which proved that the near surface region of irradiated YSO sample can efficiently support single mode propagation. After microstructural, mechanical and optical properties

Please cite this article in press as: H.-L. Song et al., Microstructural, mechanical and optical properties research of a carbon ion-irradiated Y_2SiO_5 crystal, Nucl. Instr. Meth. B (2017), http://dx.doi.org/10.1016/j.nimb.2017.01.038

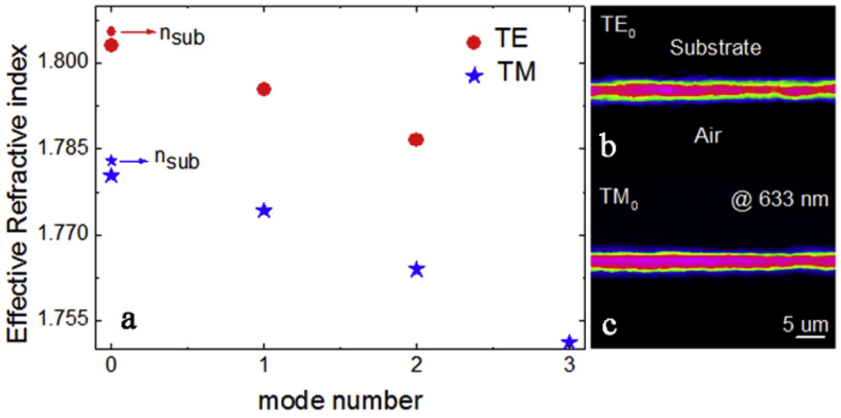

Fig. 8. (a) The effective refractive index (n_{eff}) for the transverse magnetic (TM) mode and the transverse electric (TE) mode verse mode number of the YSO virgin and planar waveguide at a wavelength of 633 nm; the near field light intensity profile of the YSO planar waveguide: (b) TE_0 mode and (c) TM_0 mode capture with a CCD camera.

research, we can find that the C ion irradiated YSO can be used as a waveguide structure. But the irradiation process and the waveguide formation mechanism still need further studies.

Acknowledgments

This work is supported by the National Natural Science Foundation of China (No. U1432120, No. 11275117), and the State Key Laboratory of Nuclear Physics and Technology at Peking University. The ToF-SIMS measurement was performed at EMSL, a national scientific user facility sponsored by the Department of Energy's Office of Biological and Environmental Research located at PNNL.

References

[1] G. Ramakrishna, H. Nagabhushana, D.V. Sunitha, S.C. Prashantha, S.C. Sharma, B.M. Nagabhushana, Spectrochim. Acta A: Mol. Biomol. Spectrosc. 127 (2014) 177.
[2] H. Jiao, X. Gao, F. Wang, A. Wu, T. Han, J. Alloys Compd. 493 (2010) 427.
[3] E. Coetsee, J.J. Terblans, H.C. Swart, J. Lumin. 126 (2007) 37.
[4] A.H.G. de Mesquita, A. Bril, Mater. Res. Bull. 4 (1969) 643.
[5] E. García, P. Miranzo, M.I. Osendi, J. Therm. Spray Technol. 22 (2013) 680.
[6] J. Felsche, Struct. Bonding (Berl.) 13 (1973) 99.
[7] C. Cannas, M. Mainas, A. Musimu, G. Piccaluga, A. Speghini, M. Bettinelli, Opt. Mater. 27 (2005) 1506.
[8] D.W. Cooke, J.K. Lee, B.L. Bennett, J.R. Groves, L.G. Jacobsohn, E.A. MicKigney, R. E. Muenchausen, M. Nastasi, K.E. Sickafus, M. Tang, J.A. Valdez, J.Y. Kim, K.S. Hong, Appl. Phys. Lett. 88 (2006) 103108.
[9] C. Li, C. Wyon, R. Moncorgé, IEEE J. Quantum Electron. 28 (1992) 1209.
[10] C.K. Lin, H. Wang, D.Y. Kong, M. Yu, X.M. Liu, Z.L. Wang, J. Lin, Eur. J. Inorg. Chem. 18 (2006) 3667.
[11] L. Wang, K.M. Wang, F. Chen, X.L. Wang, L.L. Wang, H. Liu, Q.M. Lu, Opt. Express 15 (2007) 16880–16885.
[12] J.L. Jackel, C.E. Rice, J.J. Veselka, Appl. Phys. Lett. 41 (1982) 607–608.
[13] Y.L. Lee, Y.C. Noh, C.S. Jung, T.J. Yu, B.A. Yu, J.M. Lee, D.K. Ko, Appl. Phys. Lett. 86 (2005) 011104.
[14] F. Chen, X.L. Wang, K.M. Wang, Opt. Mater. 29 (2007) 1523.
[15] X.L. Wang, K.M. Wang, F. Chen, G. Fu, S.L. Li, H. Liu, L. Gao, D.Y. Shen, H.J. Ma, R. Nie, Appl. Phys. Lett. 86 (2005) 041103.
[16] N. Kukharchyk, S. Pal, J. Rödiger, A. Ludwig, S. Probst, A.V. Ustinov, P. Bushev, A. D. Wieck, Phys. Status Solidi R 8 (2014) 880–884.
[17] P.C. Ricci, C.M. Carbonarot, R. Corpino, C. Cannas, M. Salis, J. Phys. Chem. C 115 (2011) 16630–16636.
[18] T. Kärner, V. Laguta, M. Nil, S. Zazubovich, Phys. Status Solidi B 251 (2014) 741–747.
[19] G. Corrielli, A. Seri, M. Mazzera, R. Osellame, H.D. Riedmatten, Phys. Rev. Appl. 5 (2016) 054013.
[20] A.M. Belu, D.J. Graham, D.G. Castner, Biomaterials 24 (2003) 3635.
[21] Z.H. Zhu, Y.F. Zhou, P.F. Yan, R.S. Vemuri, W. Xu, R. Zhao, X.L. Wang, S. Thevuthasan, D.R. Baer, C.M. Wang, Nano Lett. 15 (2015) 6170.
[22] J.F. Ziegler, Computer Code, SPIM, Available from <http://www.srim.org>.
[23] P. Liu, Y. Zhang, H. Xue, K. Jin, M.L. Crespillo, X. Wang, W.J. Weber, Acta Mater. 105 (2016) 429.
[24] L. Sagalowicz, G.R. Fox, J. Mater. Res. 14 (1999) 1876–1885.
[25] H. Kim, J.S. Horwitz, W.H. Kim, A.J. Mäkinen, Z.H. Kafafi, D.B. Chrisey, Thin Solid Films 1539 (2002) 420–442.
[26] M.A. Myers, M.T. Myers, M.J. General, J.H. Lee, L. Shao, H. Wang, Appl. Phys. Lett. 101 (2012) 112101.
[27] S. Maat, A.J. Kellock, D. Weller, J.E.E. Baglin, E.E. Fullerton, J. Magn. Magn. Mater. 265 (2003) 1.
[28] B. Panigrahy, M. Aslam, D. Bahadur, Appl. Phys. Lett. 98 (2011) 183109.
[29] P.K. Sharma, R.K. Dutta, A.C. Pandey, J. Magn. Magn. Mater. 321 (2009) 4001–4005.
[30] G.A. Baratta, M.M. Arena, G. Strazzulla, L. Colangeli, V. Mennella, E. Bussoletti, Nucl. Instr. Meth. B 116 (1996) 195.
[31] L.H. Zheng, G.J. Zhao, C.F. Yan, X.D. Xu, L.B. Su, Y.J. Dong, J. Xu, J. Raman Spectrosc. 38 (2007) 1421.
[32] S. Mathew, B. Satpati, B. Joseph, B.N. Dev, R. Nirmala, S. Malik, R. Kesavamoorthy, Phys. Rev. B 75 (2007) 075426.
[33] C.Y. Jin, H. Kim, S. Park, C.M. Lee, J. Alloy. Compd. 541 (2012) 163.
[34] X.M. Liu, M.L. Flem, J.L. Bèchade, I. Monnet, J. Nucl. Mater. 401 (2010) 149.
[35] Q. Huang, H. Han, R.D. Liu, G.H. Lei, L. Yan, J. Zhou, Q. Huang, Acta Mater. 110 (2016) 1.

Please cite this article in press as: H.-L. Song et al., Microstructural, mechanical and optical properties research of a carbon ion-irradiated Y_2SiO_5 crystal, Nucl. Instr. Meth. B (2017), http://dx.doi.org/10.1016/j.nimb.2017.01.038